ARL-TR-9040 ● SEP 2020

Aerodynamic Analysis of Optimized Bending Body Configurations with Trajectory Simulations

by Justin Paul, James DeSpirito, and Joseph D Vasile

Approved for public release; distribution is unlimited.

NOTICES

Disclaimers

The findings in this report are not to be construed as an official Department of the Army position unless so designated by other authorized documents.

Citation of manufacturer's or trade names does not constitute an official endorsement or approval of the use thereof.

Destroy this report when it is no longer needed. Do not return it to the originator.

ARL-TR-9040 ● SEP 2020

Aerodynamic Analysis of Optimized Bending Body Configurations with Trajectory Simulations

Justin Paul, James DeSpirito, and Joseph D Vasile
Weapons and Materials Research Directorate, CCDC Army Research Laboratory

Approved for public release; distribution is unlimited.

REPORT DOCUMENTATION PAGE	Form Approved OMB No. 0704-0188

Public reporting burden for this collection of information is estimated to average 1 hour per response, including the time for reviewing instructions, searching existing data sources, gathering and maintaining the data needed, and completing and reviewing the collection information. Send comments regarding this burden estimate or any other aspect of this collection of information, including suggestions for reducing the burden, to Department of Defense, Washington Headquarters Services, Directorate for Information Operations and Reports (0704-0188), 1215 Jefferson Davis Highway, Suite 1204, Arlington, VA 22202-4302. Respondents should be aware that notwithstanding any other provision of law, no person shall be subject to any penalty for failing to comply with a collection of information if it does not display a currently valid OMB control number.
PLEASE DO NOT RETURN YOUR FORM TO THE ABOVE ADDRESS.

1. REPORT DATE *(DD-MM-YYYY)*	2. REPORT TYPE	3. DATES COVERED (From - To)
September 2020	Technical Report	1 March 2019–31 May 2020

4. TITLE AND SUBTITLE
Aerodynamic Analysis of Optimized Bending Body Configurations with Trajectory Simulations

5a. CONTRACT NUMBER

5b. GRANT NUMBER

5c. PROGRAM ELEMENT NUMBER

6. AUTHOR(S)
Justin Paul, James DeSpirito, and Joseph D Vasile

5d. PROJECT NUMBER

5e. TASK NUMBER

5f. WORK UNIT NUMBER

7. PERFORMING ORGANIZATION NAME(S) AND ADDRESS(ES)
CCDC Army Research Laboratory
ATTN: FCDD-RLW-LE
Aberdeen Proving Ground, MD 21005-5066

8. PERFORMING ORGANIZATION REPORT NUMBER
ARL-TR-9040

9. SPONSORING/MONITORING AGENCY NAME(S) AND ADDRESS(ES)

10. SPONSOR/MONITOR'S ACRONYM(S)

11. SPONSOR/MONITOR'S REPORT NUMBER(S)

12. DISTRIBUTION/AVAILABILITY STATEMENT
Approved for public release; distribution is unlimited.

13. SUPPLEMENTARY NOTES
ORCID IDs: Justin Paul, 0000–0003–4133–7585; Joseph Vasile, 0000–0003–3812–6277

14. ABSTRACT
A bending-body design of the Air Force Finner projectile was investigated as a maneuver technology using Euler and Navier–Stokes simulations, as well as an optimization algorithm. A strictly bent-nose configuration was selected for focused investigation, the results of which informed the setup and execution of the optimization studies. The optimization studies identified similar optimal configurations—all strictly bent-body configurations—for each Mach number investigated (2.0, 2.5, and 3.0). The strictly bent-nose configuration was simulated in coupled Navier–Stokes trajectory simulations, which found up to 60 g of maneuver authority. Strictly bent-nose and strictly bent-body configurations as well as hybrid options were found to have similar performance with niche advantages in different ways that could be selected as control technology for extreme maneuvers.

15. SUBJECT TERMS
guided munitions, aerodynamics, computational fluid dynamics, CFD, particle swarm optimization, PSO, articulating nose

16. SECURITY CLASSIFICATION OF:			17. LIMITATION OF ABSTRACT	18. NUMBER OF PAGES	19a. NAME OF RESPONSIBLE PERSON
a. REPORT	b. ABSTRACT	c. THIS PAGE			Justin Paul
Unclassified	Unclassified	Unclassified	UU	49	19b. TELEPHONE NUMBER (Include area code) (410) 306-0797

Standard Form 298 (Rev. 8/98)
Prescribed by ANSI Std. Z39.18

Contents

List of Figures

List of Tables

Acknowledgments

The authors thank Dr Sidra Silton for assistance in the course of this study. Computational resources were provided in part by the US Department of Defense High Performance Computing Modernization Program at the US Army Combat Capabilities Development Command Army Research Laboratory Supercomputing Resource Center, Aberdeen Proving Ground, Maryland.

1. Introduction

Small-diameter gun-launched munitions with fast and aggressive maneuver capabilities are of great research interest in the ballistics community. Specifically, there has been growing interest to improve the precision and accuracy of munitions delivery to minimize collateral damage and maximize lethal effects. One method that can potentially achieve the necessary aggressive maneuver capability is bending-body technology.

Conventional maneuvering munitions rely on actuators such as canards, fins, reaction control jets, or thrust vector control to provide the control authority necessary to perform maneuvers. For canard-controlled gun-launched munitions, two configurations have typically been considered for maneuver control: 1) slowly rolling munitions equipped with a single plane of movable lifting surfaces[1] and 2) nonrolling munitions with dual-plane, movable lifting surfaces.[2] Canards have proven effective for some missions and maneuvers but can be limited in aggressive maneuvers. Bending-body technology offers a form of morphing airframe technology that can provide another method for control.[3,4] The bending-body concept may provide increased maneuver capability compared with conventional canards, which are subject to loss of effectiveness at moderate angle of attack, α, due to stall effects. Additionally, the interference loads that occur on the tail fins due to the interaction of vortices shed from the canard tips have been shown to limit maneuverability or adversely affect control.[5] However, there are concerns for the actual implementation of bending-body technology. While the projectile would fly in a straight configuration for most of the flight envelope, there is a significant increase in drag coefficient, C_D, during the maneuvering phase of flight (i.e., when the projectile is bent) that decreases performance.[3,4] Additionally, the center of pressure of the projectile may shift significantly when bent, causing destabilization of the projectile.[3,4]

Previous research on bending-body technology has focused on deflecting just the nose section of the projectile at its base, usually called deflected- or articulating-nose control. In the early 1980s, Thomson considered an articulating-nose concept, where the weapon forebody is angularly deflected about a suitable pivot point to control a tube-launched weapon.[6,7] Through his analyses Thomson found that the articulating nose does not perform well at subsonic speeds but is feasible in the supersonic regime. Landers et al.[8] performed wind tunnel tests at Mach 3 and Mach 6 on a hypervelocity projectile with an articulating nose, comparing pitch control effectiveness with a canard configuration of the same projectile. They found that the projectile with articulating-nose control reduced the forebody C_D by 5% and 13% at Mach 3 and 6, respectively. This reduction was attributed to the elimination

of the control surfaces. They also found that the reduction in axial force was increased to 10% (Mach 3) and 30% (Mach 6) at trim conditions when both control types provide similar maneuverability. Interference effects were found on both the articulating-nose and canard-controlled noses but at low α (<6°). Vaughn and Auman[9] demonstrated capability to model the same deflected-nose concept using the Cartesian-grid Euler (inviscid) computational fluid dynamics (CFD) solver Cart3D.[10] Shoesmith et al.[11] performed CFD simulations of the same deflected-nose projectile using the parabolized Navier–Stokes equations and found that the downstream flow was insensitive to the nose deflection, providing an opportunity to decouple responses of nose control and fin-mounted actuators. They also determined that the estimated actuator loads could be met with current actuators.

Young and Silton[4] demonstrated multiple bends could increase the advantage in control authority but at the cost of increased C_D. Paul and Silton[3] found that the C_D at $\alpha = 0°$ for a bending-body configuration increased about 22% over that of the unbent configuration. However, this was comparable to the C_D of a canard configuration of the same missile with 10° canard deflection. Finding the "optimum" shape for a bent-body configuration leverages the control authority bending-body technology offers while mitigating the cost of increased C_D. Paul and Silton[3] demonstrated the effectiveness of using Cart3D to calculate the aerodynamic coefficients of a bent-body projectile compared with full Reynolds-averaged Navier–Stokes (RANS) CFD simulations. In 2018 Paul et al.[12] investigated the shape optimization of a bent-body projectile configuration using two different objective functions. These optimal configurations were then compared with conventional canard configurations, and it was found that the aerodynamic results suggested the bending-body configurations had advantages.

The US Air Force Academy has also recently investigated articulating-nose concepts in both supersonic and subsonic Mach numbers.[13–16] Stephen et al. confirmed Thomson's results that bending-body technology is significantly less effective at subsonic Mach numbers.[13,14] However, Stephen et al. also found that strakes, canards, and other control surfaces can improve the effectiveness of bending-body technology across multiple Mach numbers.[15,16] In addition to making this discovery in the subsonic regime, it was also discovered that control surfaces, such as strakes, are able to generate synergistic effects with articulating-nose technology in the supersonic regime that were found superior to either articulating-nose technology or control surfaces implemented individually. Stephen et al. also studied two methods of bending, straight and smooth (parabolic), to find that straight bending is somewhat superior to smooth bending.[14] Stephen et al. confirmed that articulating-nose technology is more effective in supersonic flight as low as Mach 2.0.[16] Another significant result the US Air Force Academy

discovered is the significance of orienting control surfaces when implementing articulating-nose technology. The "+" orientation produces greater pitching moment than the "X" orientation but less lateral stability. Lateral forces were found to be significant due to asymmetric vortices produced by the ogive section of the geometry,[14,15] which was previously observed by Thomson.[6,7]

Previous work by the authors of this report, summarized in 2019 by Paul et al.,[17] demonstrated the bending-body approach as a technique for aerodynamic control, confirmed the viability of inviscid Cart3D predictions as a method to assess the aerodynamics of a bent-body configuration, and compared two different particle swarm optimization (PSO) algorithms. The current investigation continues the research performed by Paul et al.[12,17] The two optimal individuals found in that study (at Mach 2.0) were considered for further analysis. An equivalent cumulative bending-angle, bent-nose configuration was investigated with RANS CFD predictions. These investigations led to the expansion of the α range considered previously,[3,4,12] as it was discovered that configurations previously found "to not trim" did in fact reach a trimmed condition at higher α. This resulted in additional configurations that could be included in the consideration for optimal configuration. The same PSO algorithm[18] was again implemented, expanding the range of α for the previous optimization study. With the extended α range, the optimization goal of maximizing pitching moment at $\alpha = 0°$ (C_{m_0}) was trivial. Therefore, the only optimization goal considered in the current investigation is to maximize lift-to-drag ratio (*L/D*) at trim angle of attack, α_t. The optimization studies in the current paper were conducted for Mach numbers of 2.0, 2.5, and 3.0. Coupled, six-degree of freedom (6-DOF) trajectory simulations using a fully viscous RANS CFD solver were also completed. The trajectory simulations provided an improved understanding of how the perceived advantages from the steady-state aerodynamics produce actual advantages in control authority.

2. Approach

2.1 Air Force Finner

The Air-Force Finner (AFF) projectile[19] was used as the baseline geometry (Fig. 1). This projectile was chosen because it has been studied extensively, with a large volume of computational and empirical data available for comparison. The projectile has four uncanted, clipped delta tail fins spaced equidistant circumferentially. The AFF has a length-to-diameter, or fineness, ratio of 10, and the nose cone length is 2.5 *D* (diameter, *D* = 30 mm). The center of gravity (CG) is 4.8 *D* from the tip of the nose. The fins are beveled on the leading and trailing edges with a root chord of 4/3 *D* and a semi-span of 0.5 *D*. The mass of the projectile

was 664.3 g, the axial mass moment of inertia, I_{xx}, was 719.66 g/cm^2 and the transverse mass moments of inertia, I_{yy}, and I_{zz}, were 48567.3 g/cm^2.

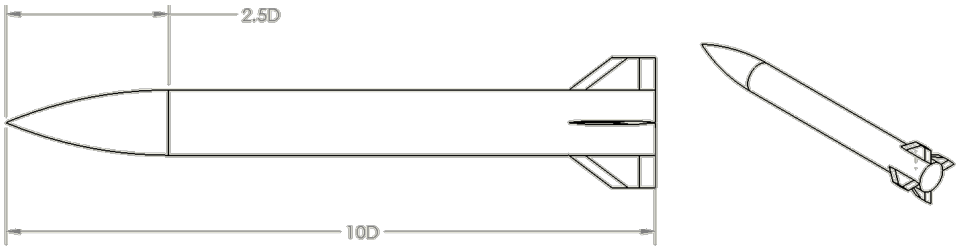

Fig. 1 Standard (unbent) body configuration of the AFF

The projectile is designed to fly in the standard body configuration and morph into a bent-body configuration when a maneuver is desired. Configurations in the "×" orientation (i.e., the fins rolled 45° out of the pitch plane) were exclusively considered. A generic, bent-body configuration is shown in Fig. 2 with control parameters Φ_1, Φ_2, and Q_1. The first bend angle (Φ_1) is the angle between the projectile axis in the unbent configuration and the axis of the deflected forward-body section. The second bend angle (Φ_2) is the angle between the axis of the deflected forward-body section and the axis of the projectile nose section (or ogive). The first bend is located between the projectile's CG and the base of the nose section. The location of this first bend, (Q_1), is allowed to vary between 1.0 and 61.7 mm from the CG in 8.67-mm increments. The location of the second bend angle is fixed at the base of the nose cone. The bend angles (Φ_1 and Φ_2) are permitted to vary from 0° to 7° in 1° increments. These control parameters are listed in Table 1. The angle of attack of the projectile is defined as the angle between the freestream velocity vector and the axis of the unbent projectile (dashed blue line in Fig. 2).

Table 1 Control parameter values

Φ_1(°)	0	1	2	3	4	5	6	7
Φ_2(°)	0	1	2	3	4	5	6	7
Q_1(mm)	1.00	9.67	18.33	27.00	35.67	44.33	53.00	61.67

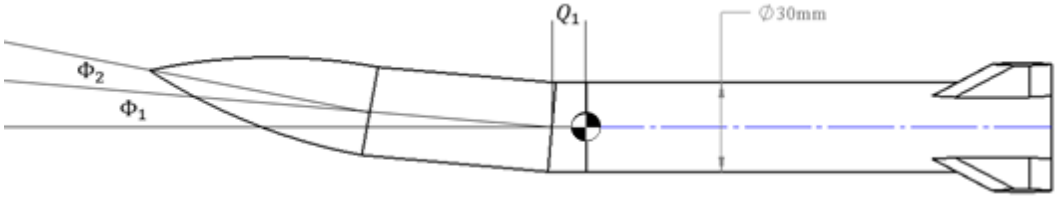

Fig. 2 Bent-body configuration of the AFF

To effectively categorize the various geometries within the design space set by the bending-body parameters, an "effective" bending angle, θ, (Fig. 3) is defined to describe the combined bending of the nose and body sections. An imaginary right triangle is defined with a vertex at the CG, and θ defined to be the angle between the horizontal line from that vertex to the nose in the unbent configuration and the hypotenuse, H, when the nose is in the bent configuration. The H dimension only decreases 1.2 mm (0.4%) as the nose changes from the undeflected to the most-deflected position.

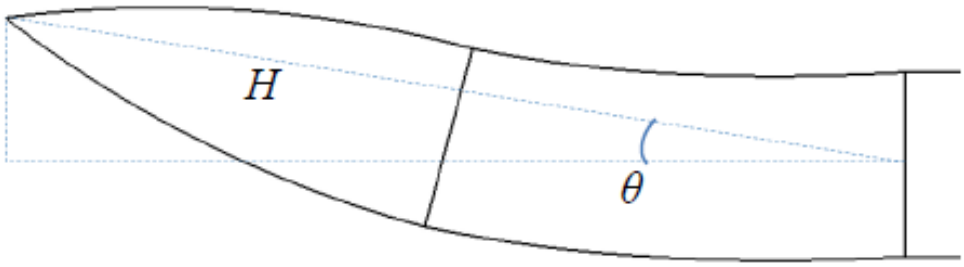

Fig. 3 Imaginary triangle characterizing the "bentness" of a generic bent body

2.2 Semi-Empirical Analysis

Missile DATCOM (release 2014)[20] is an engineering-level computer program for estimating aerodynamic stability and control characteristics of conventional missile configurations. It uses both theoretical and empirical methods to encompass the entire speed regime from subsonic to hypersonic flight. The aerodynamic forces and moments at multiple flight conditions (i.e., M_∞, α, ϕ, and δ) for a given configuration can typically be computed in a matter of seconds. Due to its limited modeling capabilities, it is the least accurate data source. Nonetheless, Missile DATCOM produces an adequate aerodynamic dataset foundation for a body-fin configuration and is assessed to provide insight into trends of the aerodynamic coefficients for a bending-body configuration across flight conditions (M_∞ and α).

2.3 Euler CFD Analysis

The computational investigations were performed using NASA's inviscid CFD package Cart3D.[10] Cart3D is a high-fidelity analysis package for aerodynamic design and analysis that includes a Cartesian mesh generator, with cut-cells near surface boundaries, and an inviscid flow solver (flowCart [fC]). For the configurations considered in Cart3D, a stereolithography geometry file generated using SOLIDWORKS[21] was used to create the surface mesh, which defines the vehicle boundaries within the Cartesian mesh after setting the domain's extent and resolution. While Cart3D includes the capability for using adaptive mesh

refinement, manual density boxes were used to refine the wake region of the projectile. The domain extended 40 *D* in all directions from the center of the projectile. The resolution was chosen such that the smallest typical cell size for the domain was 0.0067 *D* (0.2 mm). The typical computational domain consisted of approximately 3.9 million Cartesian cells.

2.4 Navier–Stokes CFD Analysis

Kestrel was developed under the US Department of Defense (DOD) High Performance Computing Modernization Program initiative to improve DOD acquisition programs through use of computational science and engineering tools.[22] The result of the initiative is called the Computational Research and Engineering Acquisition Tools and Environments (CREATE) Program, which was established in 2008. The air vehicle portion of CREATE is referred to as CREATE-AV, and the high-fidelity fixed-wing vehicle simulation tool is called Kestrel. The unstructured mesh solver, KCFD, was used in this study to perform steady-state simulations and quasi-steady angle-of-attack sweeps to obtain aerodynamic data, and coupled, 6-DOF/CFD simulations to evaluate maneuver control authority. KCFD is a finite-volume cell-centered unstructured flow solver for 2-D and 3-D domains. Meshes can be composed of cells of tetrahedrons, prisms, pyramids, and hexahedrons in 3-D or triangles and quadrilaterals in 2-D. KCFD employs the Method of Lines using a typical Godunov scheme to compute the spatial residual with second-order accuracy. Various exact and approximate Riemann schemes are available to compute the fluxes at each element face, and up to second-order accuracy in time is achieved via a subiterative point-implicit scheme. A full 3-D computational domain was implemented that consisted of about 16 million unstructured cells. The far-field boundary of the domain was about 16 *D* radially and to the rear of the projectile base.

2.5 Particle Swarm Optimization

Using similar strategies as described in Vasile et al.,[23] PSO algorithms were used to process swarms of configurations simulated by Cart3D to optimize the shape of the bent-body configuration. The PSO algorithm is part of "evolutionary programming" paradigm and the essence is that each particle in a swarm represents a design point (i.e., a solution to the problem) that can move in the given design space searching for the optimal solution as characterized by the objective function. The theory is that as the number of iterations increase, the population increases in both agreement on the best solution and objective function evaluation. The best particle in the population at the final iteration is selected as the optimized individual. The particular PSO algorithm used in this investigation was the built-in

PSO algorithm in MATLAB.[24] In this investigation, the optimization scheme sought to find a bent-body configuration with a maximum *L/D* at α_t for a given Mach number. α_t is the angle attained in the equilibrium condition where pitching moment is zero (i.e., $C_m = 0$). For this constrained optimization problem, the evaluated bent-body configurations that do not satisfy the trimmed condition are neglected. Linear interpolation was used to find the trim angle, and reverse linear interpolation was used to find the corresponding *L/D* at that interpolated trim angle.

3. Results and Discussion

3.1 Comparison of Methodologies

An investigation using the viscous flow solver Kestrel/KCFD was performed to confirm the accuracy of the inviscid CFD calculations performed earlier.[17] Missile DATCOM predictions were also performed to evaluate its effectiveness for the bent-body configuration. A strictly bent-nose configuration with a θ value, the same as the optimal configurations (i.e., $\phi_1 = 0°; \phi_2 = 8.2°$) (Fig. 4 and Table 2) in the previous study[17] was investigated. Figure 5 shows a comparison of pitching moment predicted by Missile DATCOM, Cart3D/fC, and Kestrel/KCFD at Mach 2.0, 2.5 and 3.0 over the range $-6° \leq \alpha \leq 20°$. The Kestrel/KCFD results were obtained via a quasi-steady sweep over the range $-6° \leq \alpha \leq 16°$ (18° for Mach 3.0). Missile DATCOM does not accurately predict the pitching moment, and therefore static stability, of the bent-body configuration. This result was also observed by Stephen et al., [14] finding DATCOM to be inadequate in capturing the nonlinear effects of large nose-cone deflection. Additionally, Missile DATCOM and Cart3D/fC aerodynamics predictions of several bent-nose configurations are presented in Appendix A. It was found that Missile DATCOM does predict the lift and drag of the bending-body configuration with reasonable accuracy for $-10° \leq \alpha \leq 10°$. Therefore, it can be used to get an estimate of the *L/D* of the configuration, which is a useful design parameter.

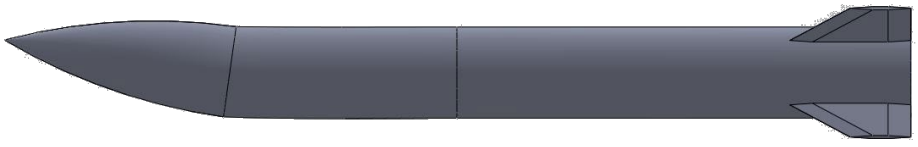

Fig. 4 Optimal C_{m_0} bent-nose configuration

Table 2 Previous optimal configurations and equivalent θ configuration at Mach 2

Configuration	Φ_1 (deg)	Φ_2 (deg)	Q_1 (mm)	θ (°)	L/D	C_{m_0}	α_t (deg)
Optimal L/D	3	2	1	4.021	1.871	0.800	9.1
Optimal C_{m_0}	1	7	53	4.107	1.749	0.819	8.8
Equivalent θ (Cart3D)	0	8.2	. . .	4.143	1.418	0.781	7.4
Equivalent θ (KCFD)	0	8.2	. . .	4.143	1.868	0.787	11.9

The Cart3D/fC predictions were found to compare reasonably well with the higher-fidelity Kestrel/KCFD predictions. Figure 5 shows that for $\alpha \leq 6°$, the Cart3D prediction of pitching moment compares very well to Kestrel/KCFD for each of the three Mach numbers. Above this $\alpha \approx 6°$, Cart3D slightly underpredicts C_m, which is likely due to less accurate prediction of separated flow on the leeward-side of the bent nose. Both predictions have the similar period of neutral stability, followed by a rapid increase in stability. The latter effect is likely a result of the nose region being stalled while the fins are not stalled (i.e., still increasing in normal force with increasing α). Although there is not a large difference between the two simulations, the value of α_t at Mach 2.0 is affected because pitching moment at "trim" in the Cart3D simulation was near zero. This results in Cart3D predicting $\alpha_t \approx 7°$ rather than $\alpha_t \approx 12°$ as predicted by Kestrel/KCFD. The trim angle becomes more defined as Mach number increases and the magnitude of the slope increases. However, the Cart3D results consistently overpredict the stability, leading to lower predicted trim angles. The differences are small and should be accounted for when determining the usual "safety factor" that should be used when using lower-fidelity analysis tools.

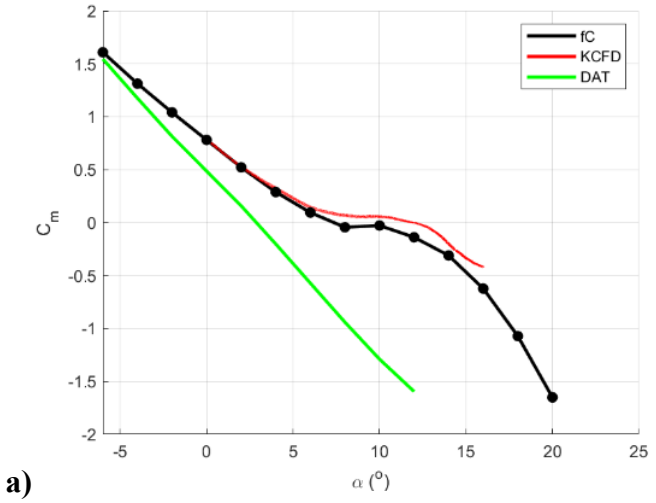

a)

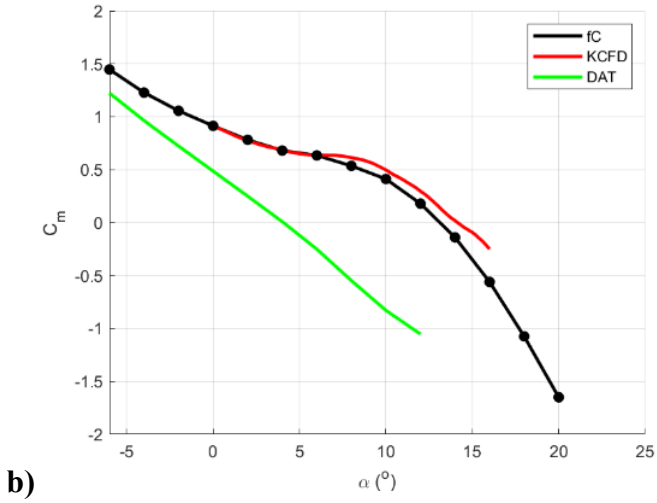

b)

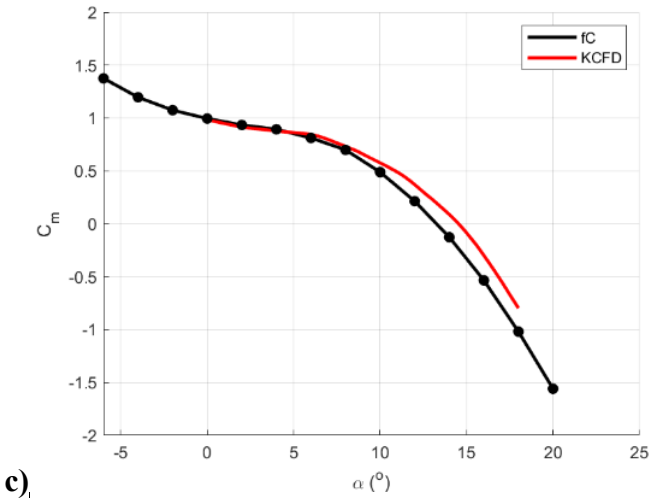

c)

Fig. 5 Pitching moment at Mach a) 2.0, b) 2.5, and c) 3.0 for strictly bent-nose configuration ($\Phi_1 = 0°; \Phi_2 = 8.2°$) predicted using fC, Kestrel/KCFD, and Missile DATCOM

Figures 6–9 present the comparison of C_D, C_L, and L/D for the four Mach numbers, 1.8, 2.0, 2.5, and 3.0. At each Mach number, Cart3D predictions of C_L and C_D, and

subsequently *L/D*, compare very well to the higher-fidelity Kestrel/KCFD predictions. The Cart3D predicted C_D is similar to the Kestrel/KCFD prediction, though the former does not include the viscous boundary layer. This is likely due to the majority of the C_D being due to the pressure component for this configuration.

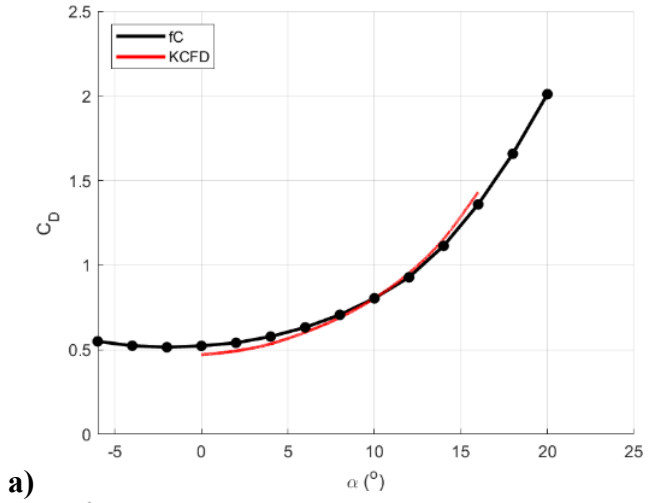

a)

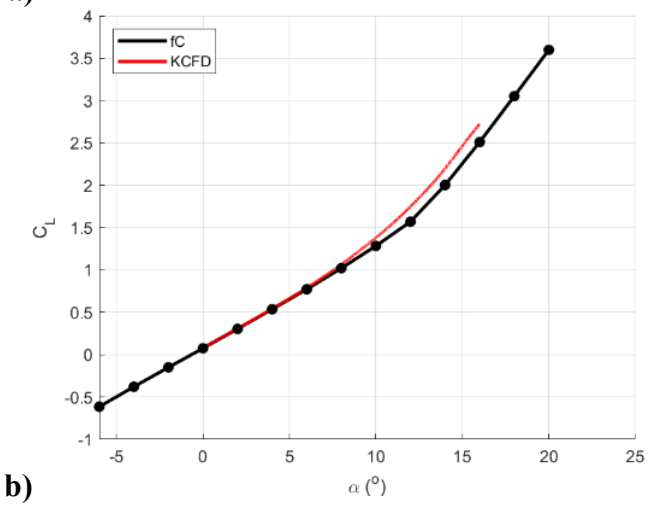

b)

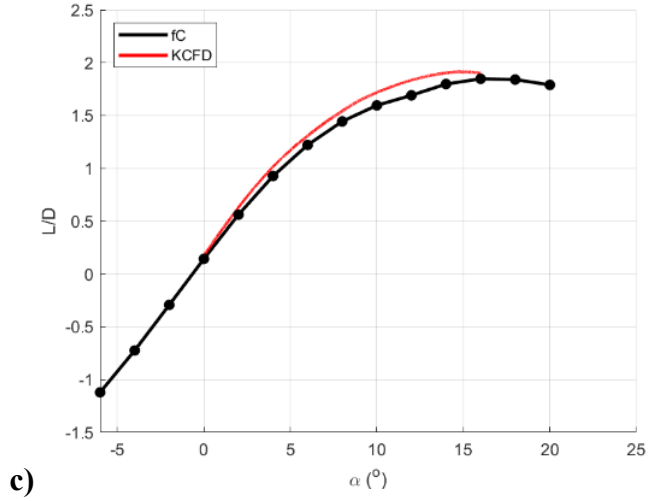

c)

Fig. 6 a) C_D, b) C_L, and c) L/D at Mach 1.8 for a strictly bent-nose configuration ($\Phi_1 = 0°; \Phi_2 = 8.2°$) predicted using fC and Kestrel/KCFD

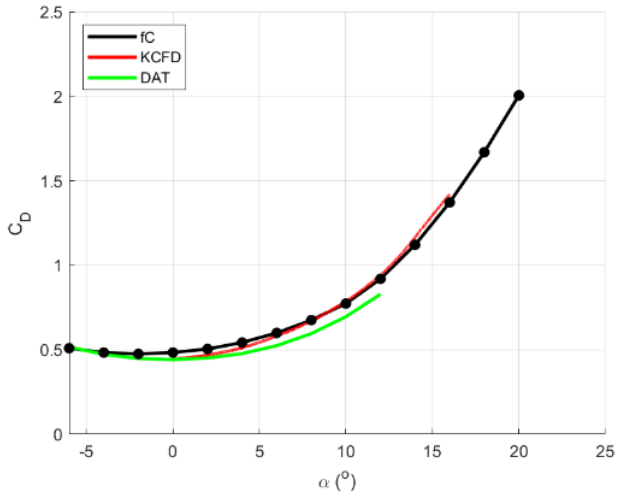

a)

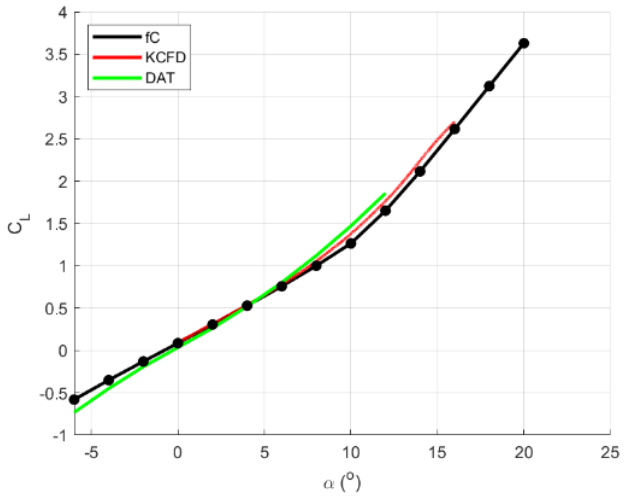

b)

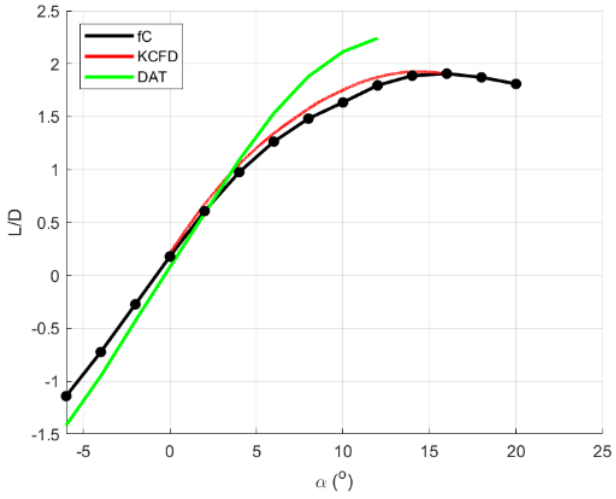

c)

Fig. 7 a) C_D, b) C_L, and c) L/D at Mach 2.0 for a strictly bent-nose configuration ($\Phi_1 = 0°; \Phi_2 = 8.2°$) predicted using fC, Kestrel/KCFD, and Missile DATCOM

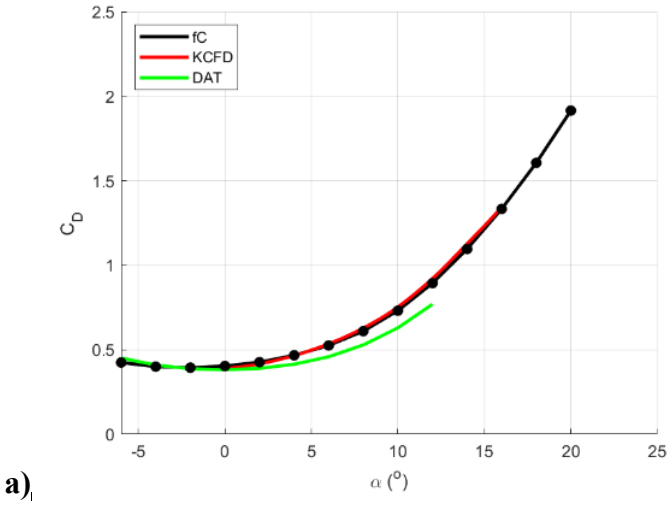

a)

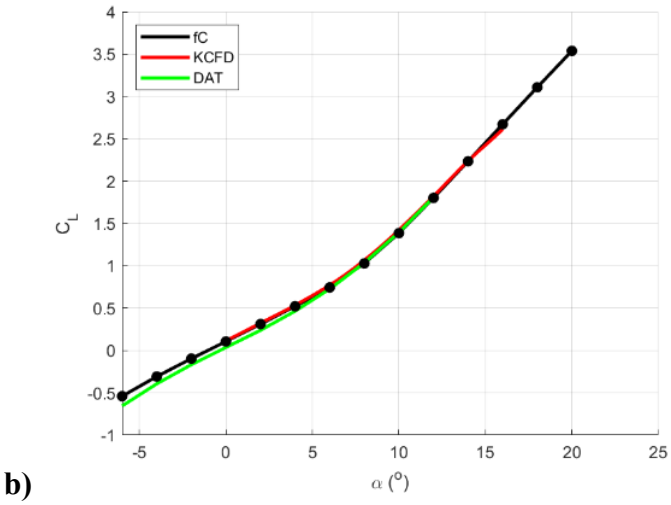

b)

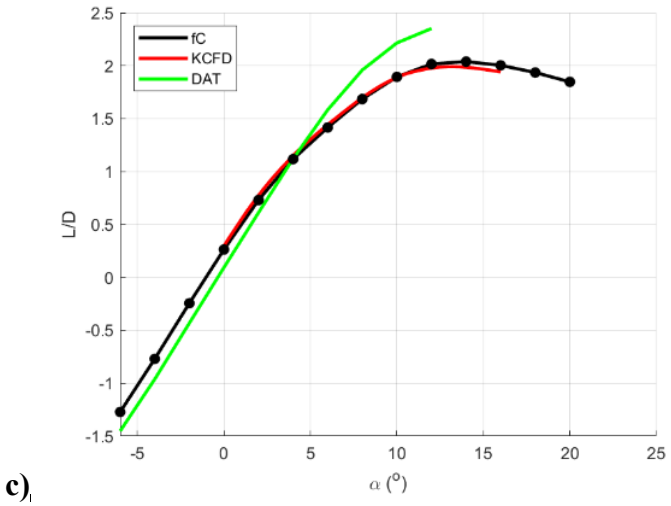

c)

Fig. 8 a) C_D, b) C_L, and c) L/D at Mach 2.5 for a strictly bent-nose configuration ($\Phi_1 = 0°; \Phi_2 = 8.2°$) predicted using fC, Kestrel/KCFD, and Missile DATCOM

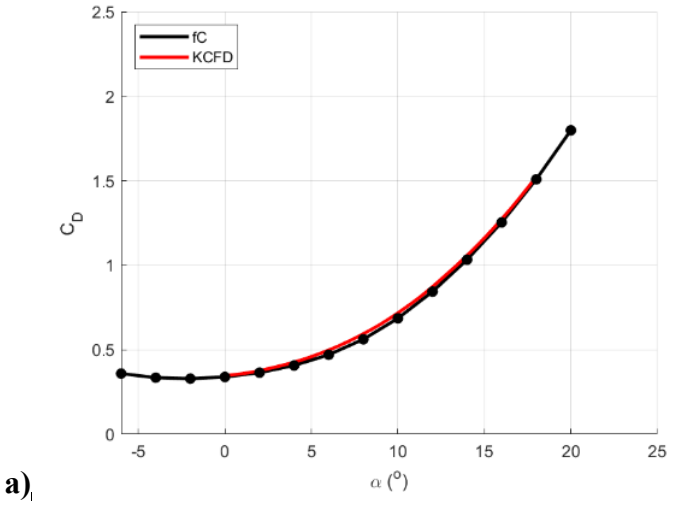

a)

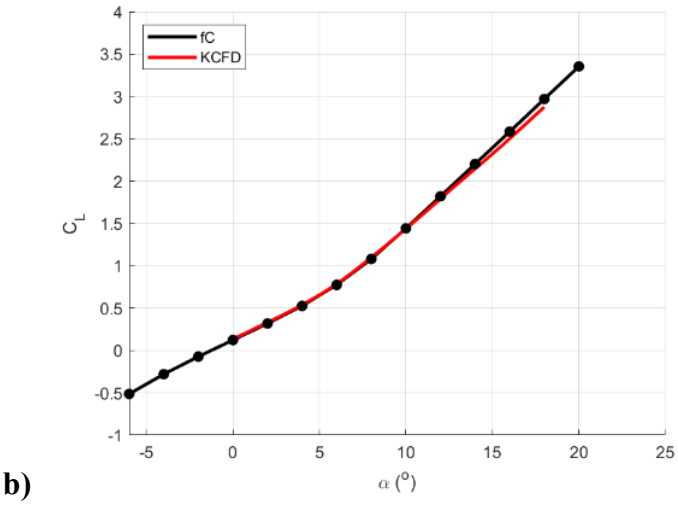

b)

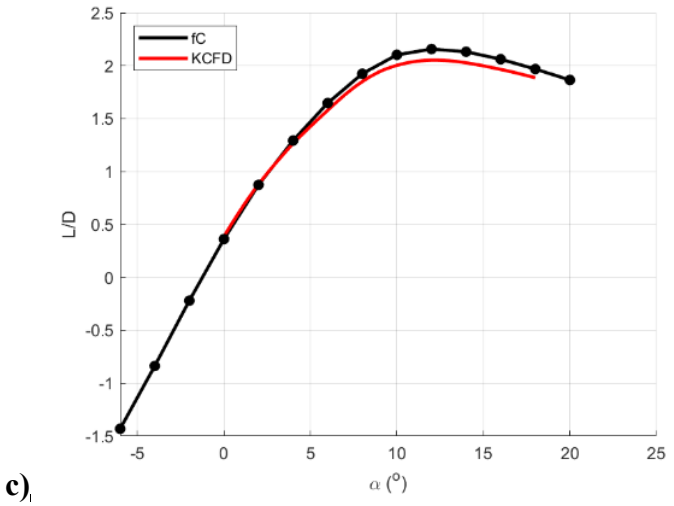

c)

Fig. 9 a) C_D, b) C_L, and c) L/D at Mach 3.0 for a strictly bent-nose configuration ($\Phi_1 = 0°; \Phi_2 = 8.2°$) predicted using fC and Kestrel/KCFD

Figures 7 and 8 show comparisons of Missile DATCOM predictions of C_L, C_D, and *L/D*. The difference in *L/D* does become larger for $\alpha > 5°$. At Mach 2.0 the difference appears to be due to differences in both the C_L and C_D predictions. However, at Mach 2.5 the differences are primarily due to differences in the C_D prediction.

3.2 Optimization Studies

The design space in the previous optimization study[17] only included $-10° \leq \alpha \leq 10°$ at Mach 2.0 and resulted in a number of configurations that did not trim (i.e., C_m did not cross zero). As shown in Fig. 5a, the configuration becomes more stable and trims at higher α. Therefore, the optimization study at Mach 2.0[17] was repeated for the maximum *L/D* at α_t objective function using the aerodynamic coefficients obtained from Cart3D. The range of α was modified to include higher values and remove some negative values from the design space. All configurations in the design space were now found to reach trimmed condition. Optimization studies were also conducted for Mach 2.5 and Mach 3.0.

The optimal configurations for each Mach number are shown in Table 3. The optimal configurations at each Mach number are all "bent-body" configurations, with the lowest option for Φ_2 (i.e., $\Phi_2 = 0$) and the Q_1 value closest to the CG.

Table 3 Optimal *L/D* configurations for different Mach numbers

Configuration	Φ_1 (deg)	Φ_2 (deg)	Q_1 (mm)	θ (deg)	*L/D*	α_t (deg)
Mach 2.0	5	0	1	4.965	1.954	13.4
Mach 2.5	4	0	1	3.972	2.145	11.4
Mach 3.0	4	0	1	3.972	2.324	11.2

The optimization results for Mach 2.5 are plotted in Fig. 10. The optimal configuration is identified with the black symbol. It is observed there are a number of configurations that have similar performance. Therefore, the configurations were categorized as strictly Bent Body (green symbols), strictly Bent Nose (red symbols), and Unknown Shape (blue symbols). The definition of each of these categories is shown in Table 4. Above $\theta \approx 2.5°$, the strictly Bent Body are better performing than the strictly Bent Nose configurations (Fig. 10a) and the difference increases with θ. Figures 10b and 10c show that while the strictly Bent Nose configurations provide more lift, the additional drag they incur leads to a reduced *L/D*. Figure 10d shows that the strictly Bent Nose configurations also trim at a larger angle for the same θ value. The strictly Bent Body configuration also reach about 31% greater than the equivalent θ than the strictly Bent Nose configurations;

however, the difference in trim angle (Fig. 10d) is only about 2°. The final strictly Bent Nose configuration appears to be an outlier. However, as this was the largest deflection investigated, it is possible that it is a real result, as no issues with convergence of the numerical solutions were found. In addition, surface pressure and flow-field contour plots of the "outlier" simulation appear reasonable compared to another strictly bent-nose configuration (see Appendix B). Note the increased L/D of this point is associated with a decrease in both C_L and C_D.

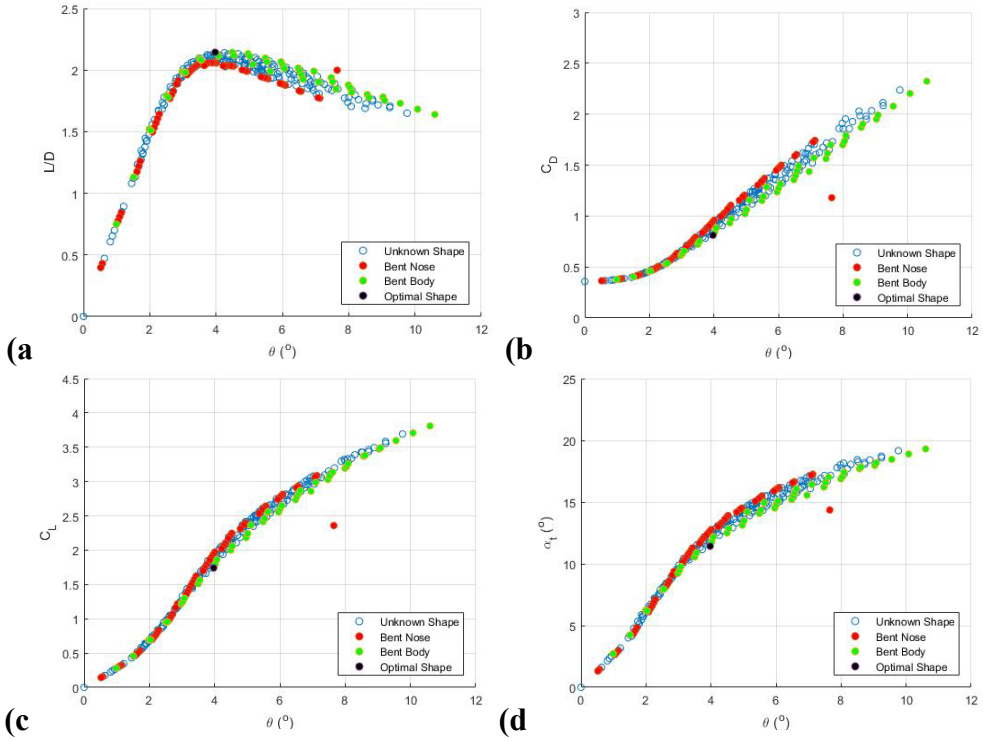

Fig. 10 a) L/D, b) C_D, and c) C_L vs. θ for each configuration at their respective trim condition, and d) α_t vs. θ for Mach 2.5

Table 4 Categories and definitions characterizing bending-body shapes

Categories	Definition
Strictly bent-body	(Q_1 = 1 mm) and ($\Phi_1 > 0°$)
Strictly bent-nose	(Q_1 = 61.67 mm) and (($\Phi_1 > 0°$) or ($\Phi_2 > 0°$))
Unknown Shape	Others not meeting these requirements

Figure 11 shows the L/D vs. θ for each configuration for Mach 2.0, 2.5, and 3.0. Similar trends are observed at each Mach number, but the difference in performance between the strictly Bent Body and strictly Bent Nose configurations increases with Mach number. It is also observed from Fig. 11 that for all Mach numbers and $\theta \leq\approx 3°$ ($\alpha_t \leq\approx 10°$), there are strictly Bent Nose and strictly Bent Body configurations that have nearly the same performance. This result indicates that

configuration design tradeoffs could be made without significantly affecting the overall performance. The results for all three Mach numbers are presented in Appendix C.

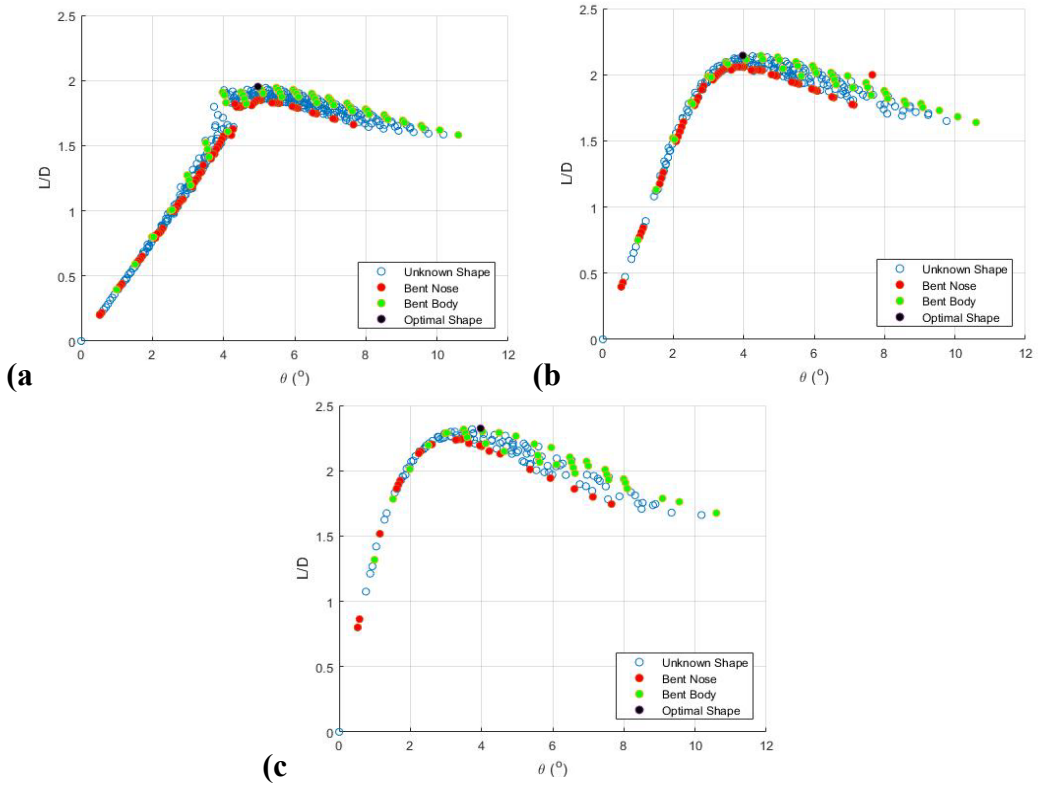

Fig. 11 L/D **for each configuration at their respective trim condition for Mach a) 2.0, b) 2.5, and c) 3.0**

3.3 Coupled Navier–Stokes Simulations with Trajectory Simulations

An investigation using Kestrel/KCFD was performed to evaluate the maneuver authority of the bent configurations via coupled 6-DOF/CFD simulations. Coupled 6-DOF simulations with an initial bend in the "up" (-z) direction of 8.2° of the nose (ogive section) were completed to better understand the benefits of using bending-body technology. The bend angle of this projectile was chosen to match the equivalent bending angle of the original optimal configurations[17] (Table 2). The mass properties of the standard (unbent) AFF were used in the 6-DOF simulation. The assumption was that the transverse moments of inertia, I_{yy} and I_{zz}, would not change significantly due to the bend. Mass property estimates from SolidWorks show that I_{xx} changed (increased) the most (as expected), but only by about 3.9%. The transverse moments of inertia changed by less than 0.25%.

Figures 12a and 12b show the total angle of attack, α_T, for trajectories with initial Mach numbers of 2.0 and 2.5, respectively. As would be expected, there is a damped, oscillatory response. In both cases, the total angle attack is approaching the respective trim angles for the Mach number at that point in the trajectory, about 5° at Mach 1.83 and about 13° at Mach 2.17, respectively.

Figure 12c and 12d show the load factor (acceleration/acceleration gravity, or g) in the maneuver (pitch) plane for both Mach numbers. As indicated in Fig. 11, *L/D* increases with Mach number, leading to an increase in maneuverability. At nearly 200-m slant range, the Mach 2.5 configuration is still providing about 60 g of acceleration while the Mach 2.0 case is only providing about 12 g. The trajectory deflections in the maneuver plane achieved in just under 200-m slant range were about 14 and 25 m at Mach 2.0 and Mach 2.5, respectively (Fig. 13). The displacements in the lateral plane were only about 1.5 and 14 cm, respectively. A more gradual (and practical) increase in nose deflection, and a control system, would likely reduce peak accelerations during the overshoot.

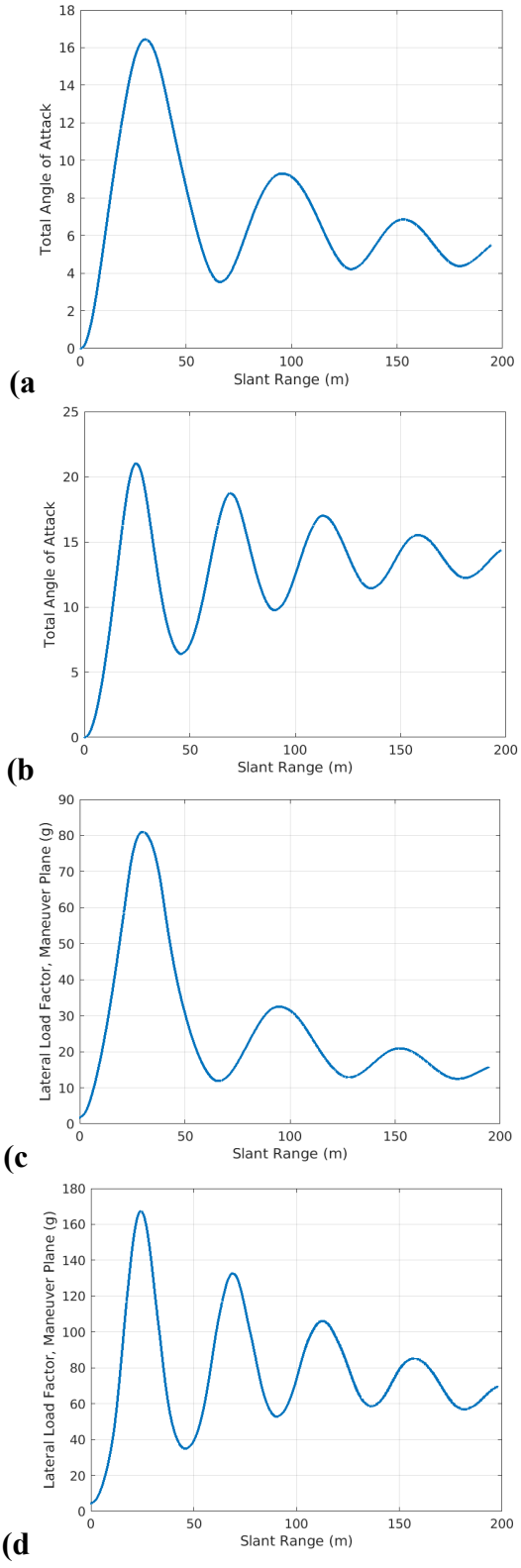

Fig. 12 Total angle of attack at Mach a) 2.0 and b) 2.5, and load factor at Mach c) 2.0 and d) 2.5

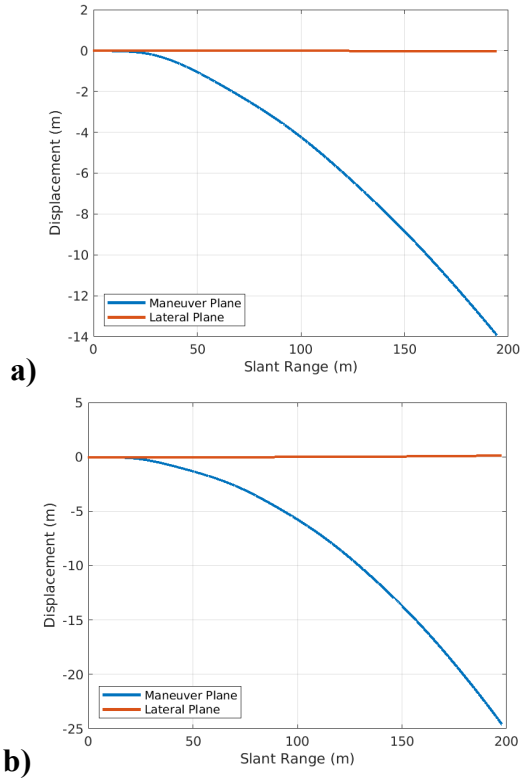

Fig. 13 Trajectory deflection at Mach a) 2.0 and b) 2.5

4. Summary and Conclusions

Two CFD simulation methodologies, Kestrel/KCFD and Cart3D were used to investigate a bending-body design of the AFF projectile. A PSO optimization algorithm was also used in conjunction with the fast Cart3D inviscid simulations. Kestrel/KCFD was used to study a strictly bent-nose configuration and comparisons with Cart3D shows that the latter, lower-fidelity prediction are very accurate up to $\alpha = 6°$. Above this angle, Cart3D accurately shows the pitching moment trend, providing a conservative estimate of stability. The Kestrel/KCFD predictions also found the configuration to trim at an angle of attack above 10°, which was the extent of the original Cart3D predictions in Paul et al.[17] This result led to the decision to extend the angle of attack range in additional optimization studies at Mach numbers 2.0, 2.5, and 3.0.

The optimization studies yielded virtually the same optimal configuration, which was a strictly bent-body configuration. However, several bending-body shapes were found to produce near optimal performance, suggesting significant design flexibility.

The strictly bent-nose configuration was then further investigated in coupled, 6-DOF/CFD Kestrel/KCFD simulations. This investigation found the strictly bent-nose configuration to have significantly enhanced maneuver capability compared with conventional control technologies, based on generated lift and pitching moment.[17] The bent-nose configuration was found to produce load factors of about 15 and 60 g for launch Mach numbers of 2.0 and 2.5, respectively. These load factors relate to displacements of about 14 and 25 m at 200-m slant range for the same respective launch Mach numbers. These results indicate that bending-body technology (including strictly bent-nose configurations) is a viable control method, from an aerodynamic perspective, for agile maneuvering munitions.

5. References

1. Fresconi FE, Harkins T. Experimental flight characterization of asymmetric and maneuvering projectiles from elevated gun firings. J Spacecraft Rockets. 2012;49(6):1120–1130.

2. Fresconi F, Celmins I, Ilg M, Maley J. Projectile roll dynamics and control with a low-cost skid-to-turn maneuver system. J Spacecraft Rockets. 2014;51(2):624–627.

3. Paul JL, Silton SI. Influence of bending locations and angles on the aerodynamic performance of a bent body projectile. Proceedings of the AIAA SciTech Forum; 2018 Jan; Kissimmee, FL. AIAA Paper No.: 2018–1269.

4. Young EB, Silton SI. Numerical study on bending-body projectile aerodynamics. Proceedings of the 34th Applied Aerodynamics Conference; 2016 June; Washington, DC. AIAA Paper No.: 2016–4331.

5. Blair AB. Wind tunnel investigation at supersonic speeds of a canard controlled missile with fixed and free-rolling tail fins. Hampton (VA): National Aeronautics and Space Administration; 1978 Sep. NASA Technical Paper No.: 1316.

6. Thomson KD. The use of a deflectable nose on a missile as a control device. Salisbury (UK): Defence Research Centre Salisbury; 1981 May. Report No.: WSRL-0211-TR.

7. Thomson KD. Wind tunnel tests on a tube-launched missile configuration with a deflectable nose control and a novel wrap-around fin stabilizer. Salisbury (UK): Defence Research Centre Salisbury; 1983 Aug. Report No.: WSRL-0327-TR.

8. Landers MG, Hall LH, Auman LM, Vaughn ME. Deflectable nose and canard controls for a fin-stabilized projectile at supersonic and hypersonic speeds. Proceedings of the 21st AIAA Applied Aerodynamics Conference; 2003 June. AIAA Paper No.: 2003-3805.

9. Vaughn ME, Auman LM. Assessment of a productivity-oriented CFD methodology for designing a hypervelocity missile. Proceedings of the 21st AIAA Applied Aerodynamics Conference; 2003 June. AIAA Paper No.: 2003-3937.

10. Aftosmis MJ, Berger MJ, Adomavicius G. A parallel multilevel method for adaptively refined Cartesian grids with embedded boundaries. Proceedings of

the 38th AIAA Aerospace Sciences Meeting and Exhibit; 2000 Jan. AIAA Paper No.: 2000-0808.

11. Shoesmith B, Birch T, Mifsud M, Meunier M, Shaw S. CFD analysis of a supersonic projectile with deflectable nose control. Proceedings of the 3rd AIAA Flow Control Conference; 2006 June. AIAA Paper No.: 2006-3200.

12. Paul JL, Vasile JD, Silton SI. Aerodynamic shape optimization of a supersonic bending body projectile. Proceedings of the AIAA Aviation Forum; 2018 June; Atlanta, GA. AIAA Paper No.: 2018-4125.

13. Stephen EJ, Abate G, McLaughlin T, Bouveret A, Laversanne D, Gerini JF, Dickinson BT. Investigation of articulating nose cone for flight control under Mach 2 conditions. Proceedings of the AIAA Aviation Forum; 2018 June; Atlanta, GA. AIAA Paper No.: 2018-3547.

14. Stephen EJ, Abate G, McLaughlin T, Figueroa M, Ringenbach S, Olivry JJ, Dickinson BT. Investigation of Mach number effects on the aerodynamic loading of an articulating nose cone missile. Proceedings of the AIAA Aviation Forum; 2019 June; Dallas, TX. AIAA Paper No.: 2019-3166.

15. Stephen EJ, Bixler B, Turner J, McLaughlin T, Dickinson B. Investigation of nose cone modifications to improve the effectiveness of an articulating nose cone on a subsonic missile. Proceedings of the AIAA Aviation Forum; 2019 June; Dallas, TX. AIAA Paper No.: 2019-3165.

16. Stephen EJ, Schlichting G, Dyke JV, Leone A, McLaughlin T. Comparison of articulating nosecones and canards for missile flight control under Mach 2 conditions. Proceedings of the AIAA Aviation Forum Virtual Event; 2020 June. AIAA Paper No.: 2020-2728.

17. Paul JL, Vasile JD, DeSpirito J, Silton SI. Aerodynamic investigation of a supersonic bending body projectile with shape optimization. Aberdeen Proving Ground (MD): CCDC Army Research Laboratory (US); 2019 Sep. Report No.: ARL-TR-8797.

18. Kennedy J, Eberhart R. Particle swarm optimization. Proceedings of the IEEE International Conference on Neural Networks; 1995; Perth, Australia. Vol. 4. p. 1942–1948.

19. Dupuis AD, Hathaway W. Aeroballistic range tests of the Air Force Finner reference projectile. Valcartier (Quebec, Canada): Defense R&D Canada; 2002 May. Report No.: TM 2002-008.

20. Rosema C, Doyle J, Blake W. Missile DATCOM user's manual – 2014 revision. Flight Dynamics Directorate, Wright Patterson Air Force Base (OH): Air Force Research Laboratory (US); 2014 Dec. Report No.: AFRL-RQ-WP-TR-2014-0281.

21. McDaniel DR, Tuckey TR. HPCMP CREATE-AV Kestrel new and emerging capabilities. Proceedings of the AIAA SciTech Forum; 2020 Jan; Orlando, FL. AIAA Paper No.: 2020-1525.

22. Dassault Systems SolidWorks Corporation. SolidWorks 2016. Waltham, MA; 2016.

23. Vasile JD, Celmins I, Nelson B. Aerodynamic design optimization of control mechanisms for a subsonic, small diameter munition. Proceedings of the AIAA Science and Technology Forum; 2018 Jan; Kissimmee, FL. AIAA Paper No.: 2018-1654.

24. MATLAB 9.0. Natick (MA): The MathWorks, Inc.

Appendix A. Additional Missile DATCOM and Cart3D Predictions

Additional Missile DATCOM and Cart3D/flowCart (fC) predictions were performed for a bent-nose only configuration ($\theta_1 = 0°; \theta_2 \neq 0°$). Missile DATCOM predictions were made for a nose deflections (ND) of $0° \leq \theta_2 \leq 8°$ and Cart3D/fC predictions were made for $0° \leq \theta_2 \leq 6°$. Figures A-1 through A-3 show Missile DATCOM provides somewhat reasonable estimates of lift and drag and their ratio. However, Missile DATCOM does not capture the nonlinear pitching moment (Fig. A-4). However, even nonlinear effects in C_L (Fig. A-1) were difficult to capture as angle of attack increases.

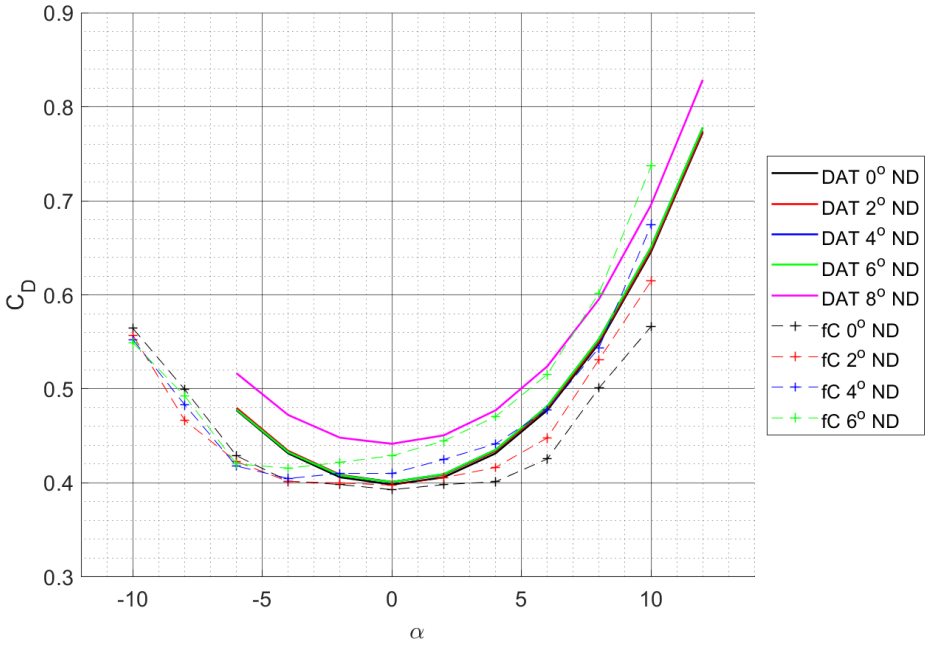

Fig. A-1 Drag coefficient at Mach 2.0 for different bent-nose deflection angles

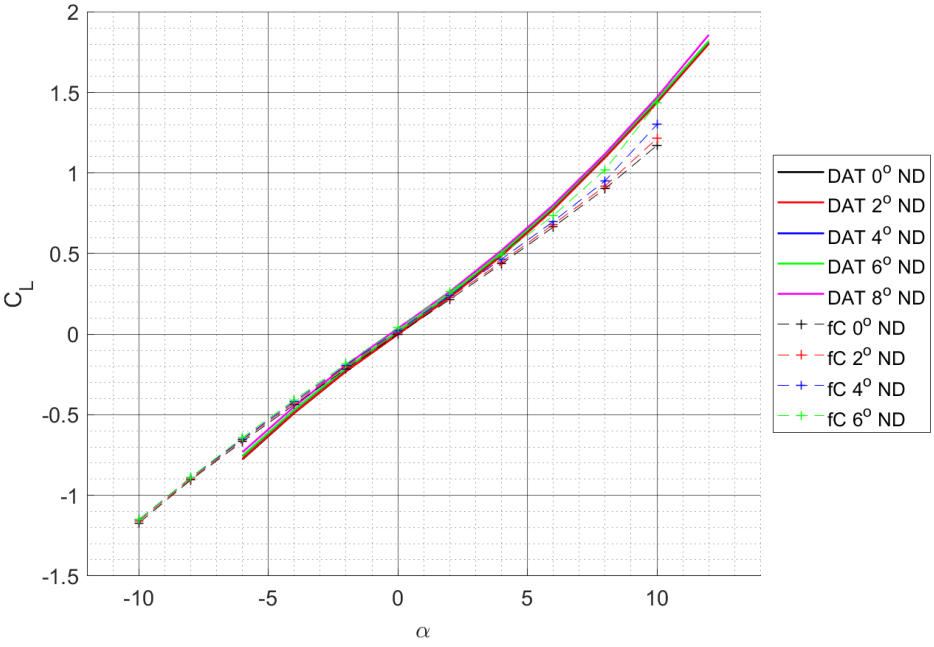

Fig. A-2 Lift coefficient at Mach 2.0 for different bent-nose deflection angles

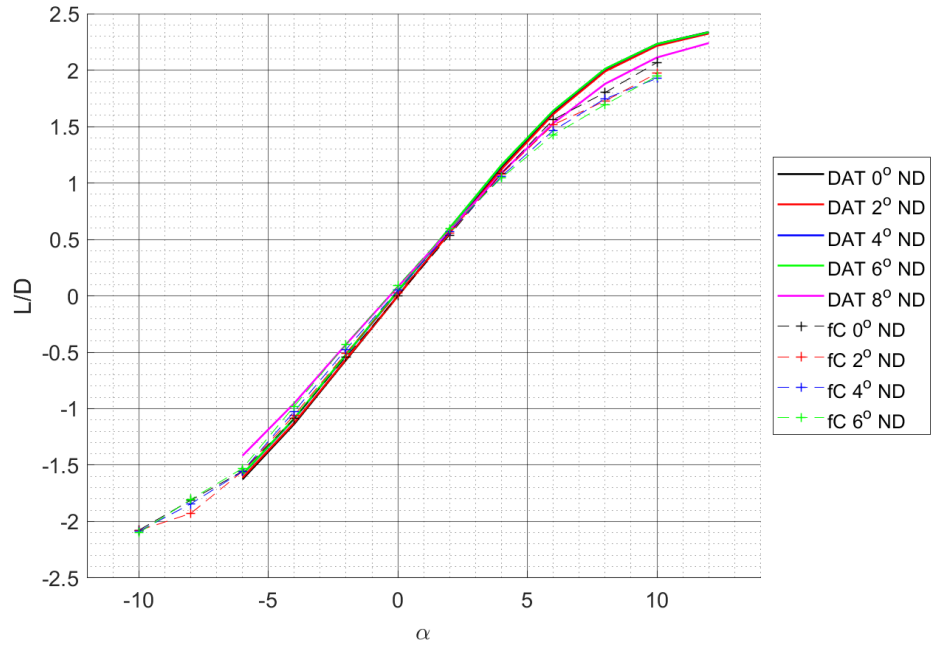

Fig. A-3 Lift-to-drag ratio at Mach 2.0 for different bent-nose deflection angles

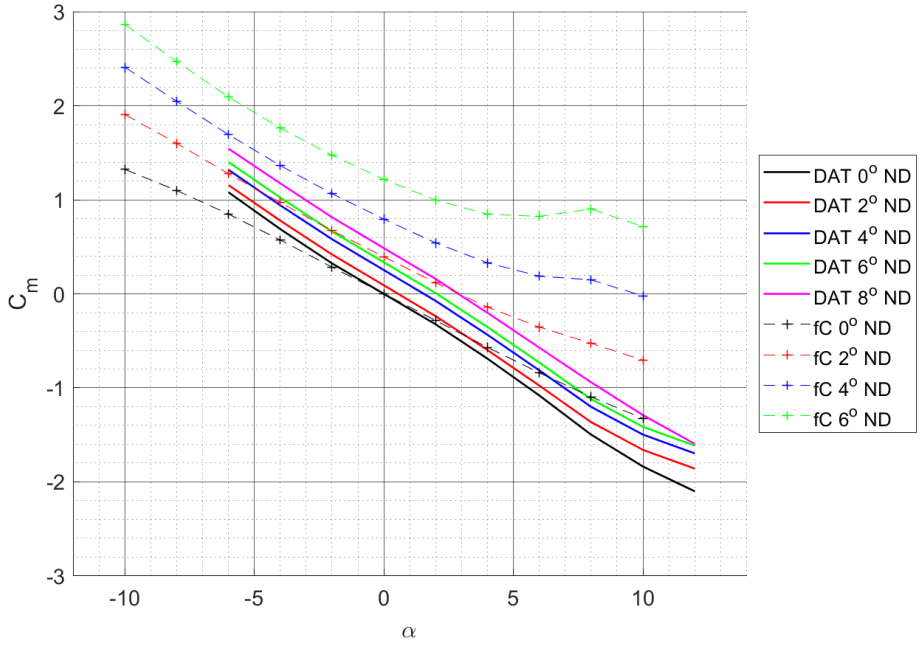

Fig. A-4 Pitching moment coefficient at Mach 2.0 for different bent-nose deflection angles

Appendix B. Strictly Bent-Nose Outlier

In Fig. B-1, there are no features of the surface pressure or Mach contours that indicate differences between the outlier configuration and a normal strictly bent-nose configuration with a slightly smaller θ value. Figure B-2, however, reveals a few distinct differences between the outlier configuration and a normal strictly bent-nose configuration. Most notably, the outlier configuration features a high-pressure region immediately behind the bent-nose section of the projectile. Most of the top surface also has generally higher pressure on the outlier configuration compared with the normal strictly bent-nose configuration. Finally, there is slightly higher pressure on the leading edge of fins for the outlier configuration. These regions of higher pressure account for the lower lift and trim angle compared with the normal strictly bent-nose configuration. These observations do not explain the abrupt change in aerodynamics from one configuration to the other, but they do indicate that simulation result for the outlier case is reasonable.

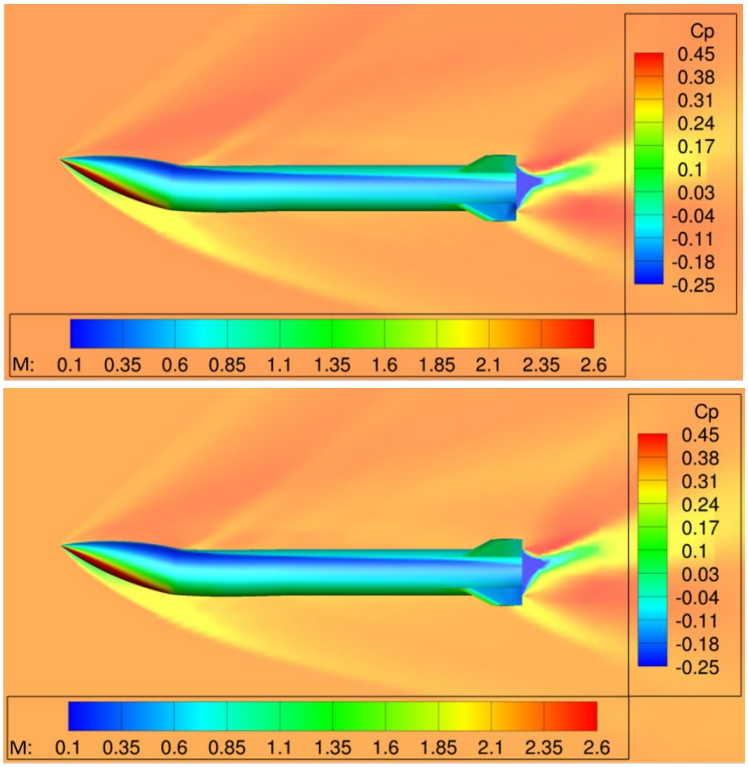

Fig. B-1 Surface pressure coefficient contour in the pitch plane of the (top) outlier configuration and (bottom) a normal strictly bent-nose configuration at Mach 2.5

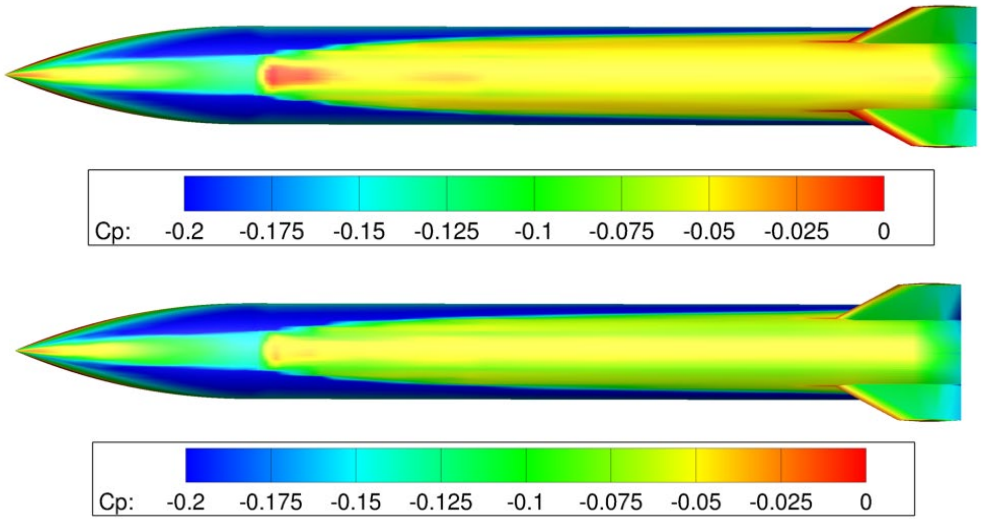

Fig. B-2 Surface pressure coefficient contour on (top) the top surface of the outlier configuration and (bottom) a normal strictly ben-nose configuration at Mach 2.5

Appendix C. Optimization Studies

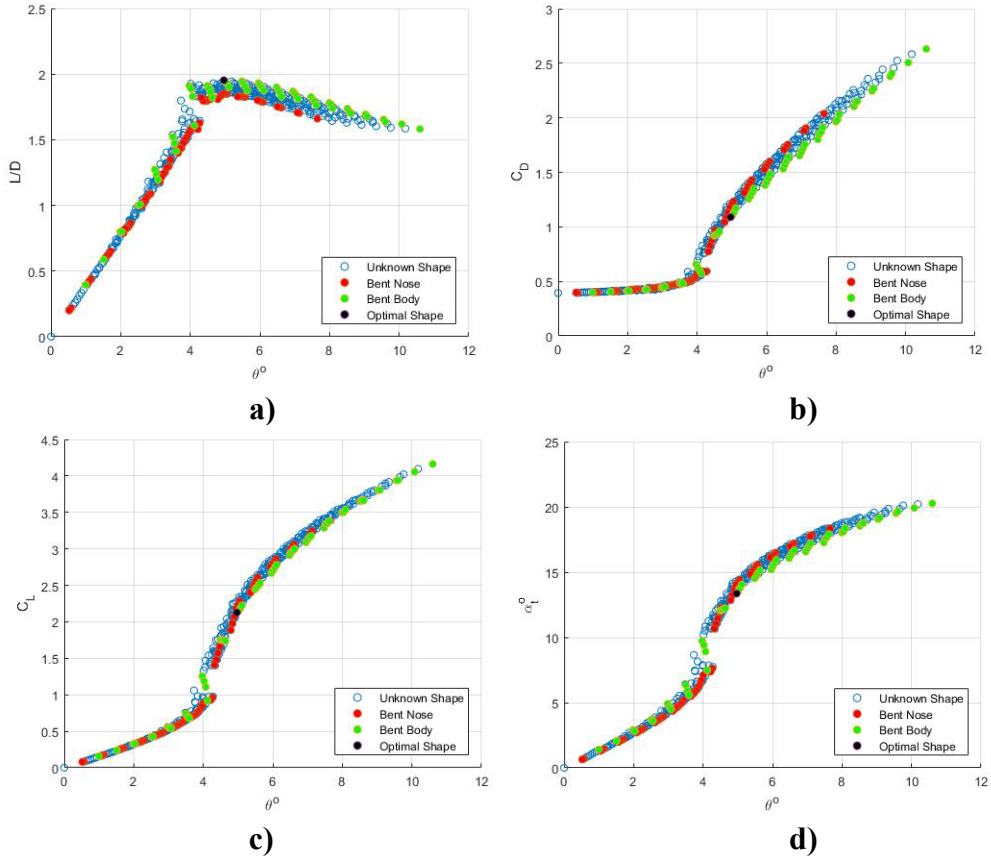

Fig. C-1 a) L/D, b) C_D, and c) C_L for each configuration at their respective trim condition, and d) α_t vs. θ for Mach 2.0

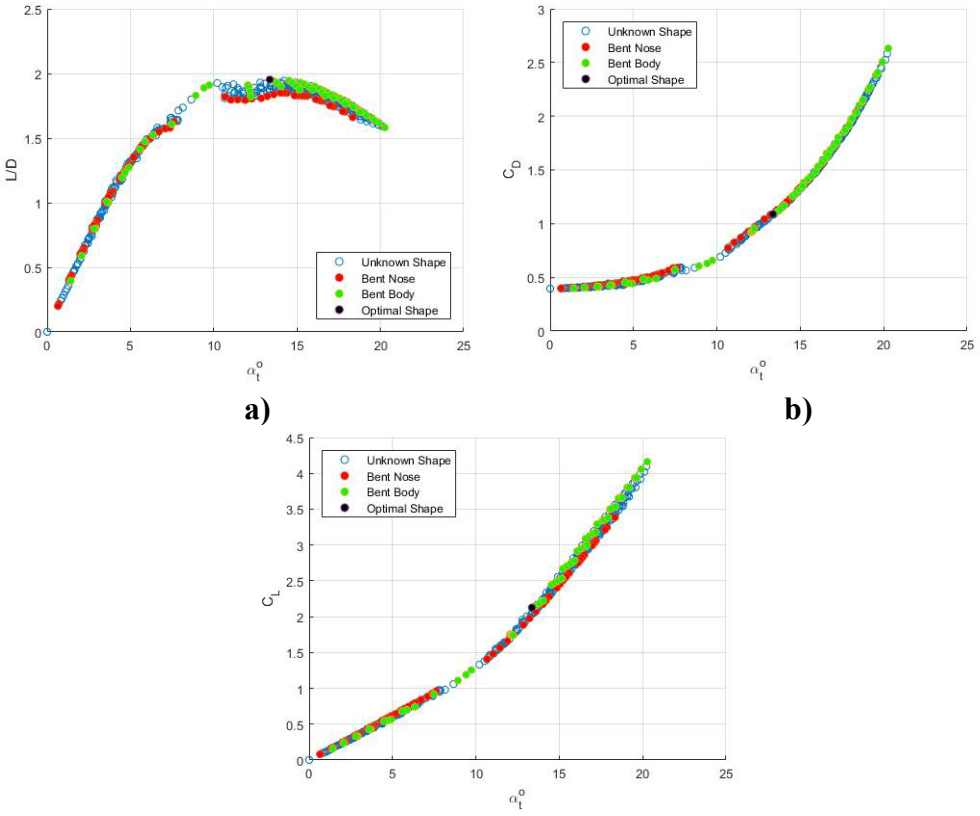

Fig. C-2 a) L/D, b) C_D, and c) C_L vs. α_t for Mach 2.0

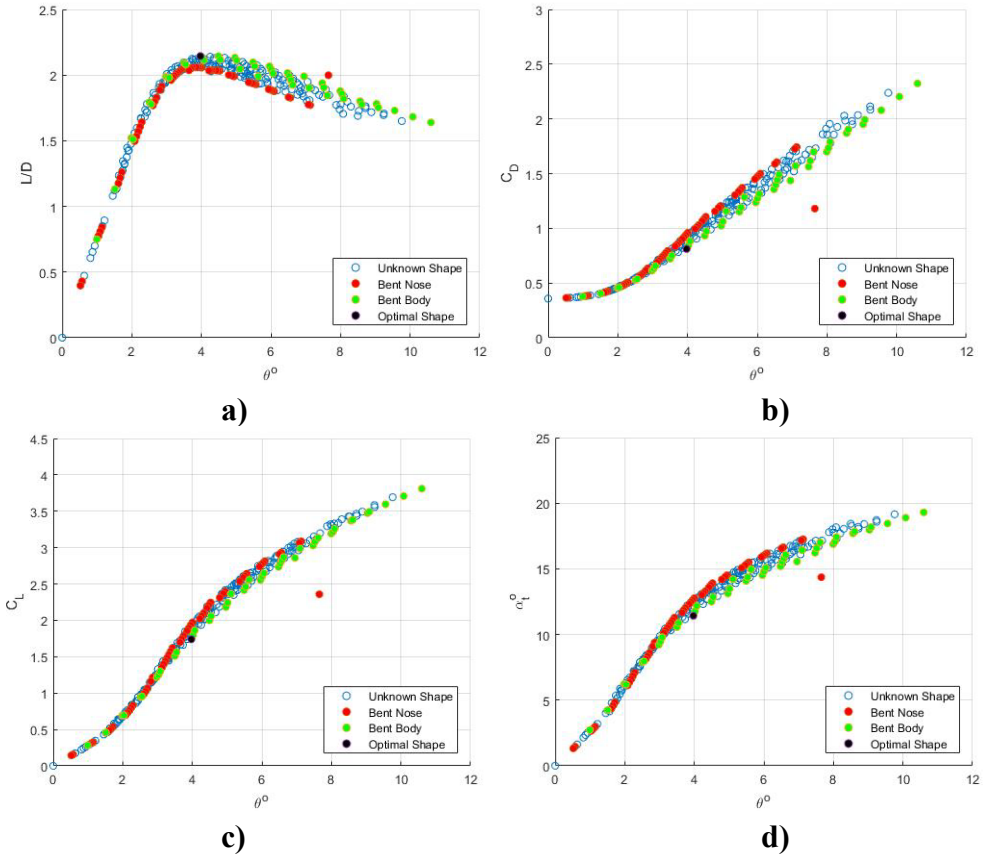

Fig. C-3 a) L/D, b) C_D, and c) C_L for each configuration at their respective trim condition, and d) α_t vs. θ for Mach 2.5

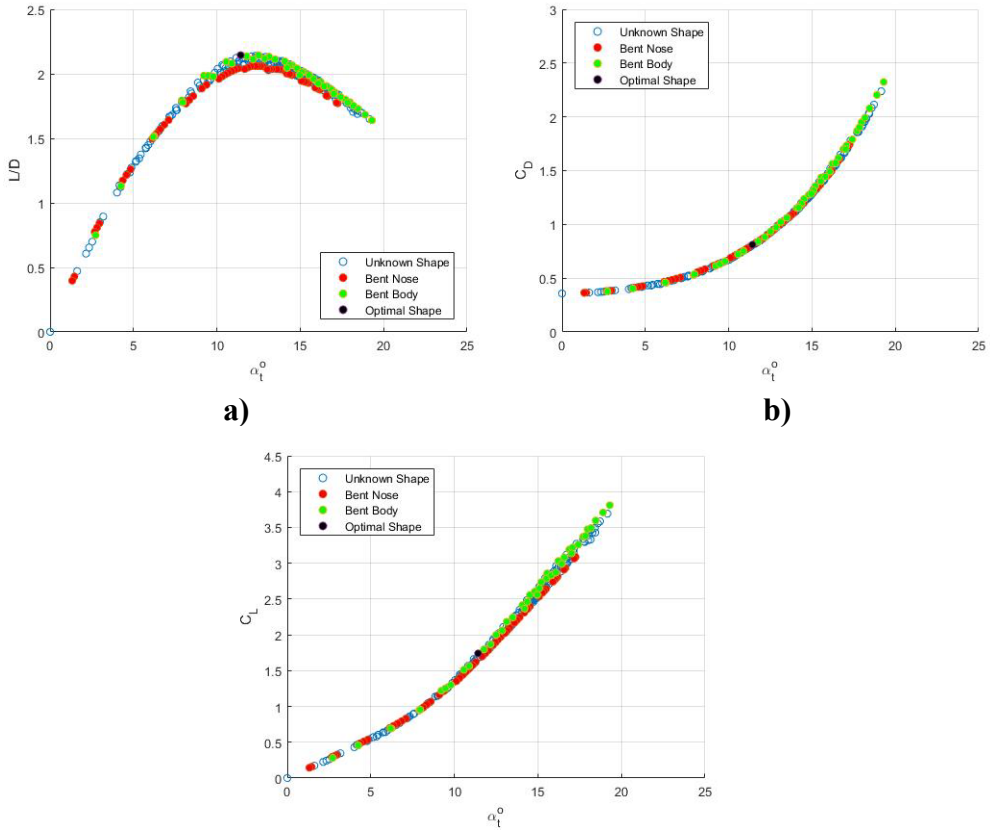

Fig. C-4 a) L/D, b) C_D, and c) C_L vs. α_t for Mach 2.5

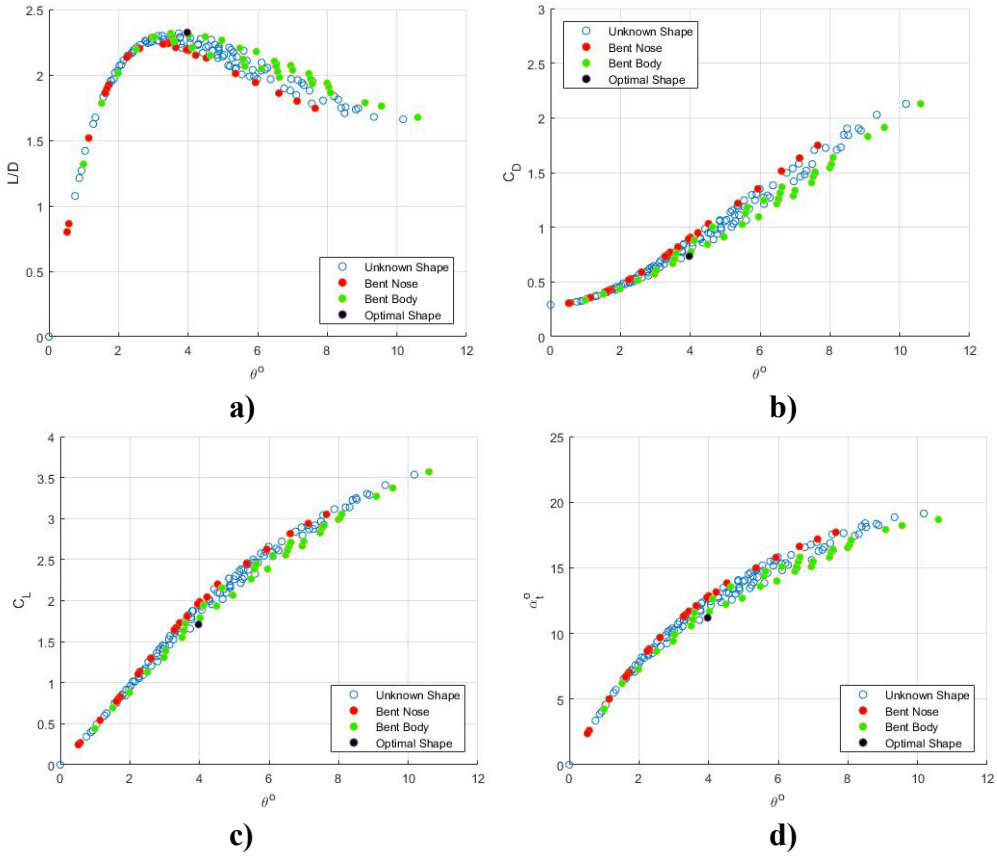

Fig. C-5 a) L/D, b) C_D, and c) C_L for each configuration at their respective trim condition, and d) α_t vs. θ for Mach 3.0

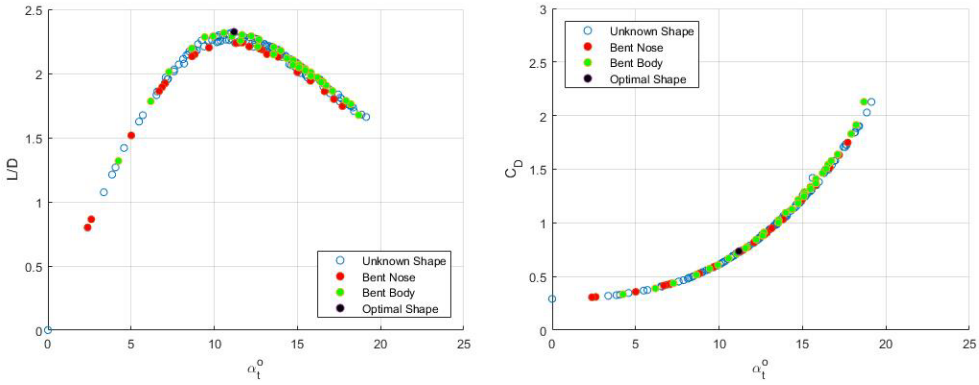

a) **b)**

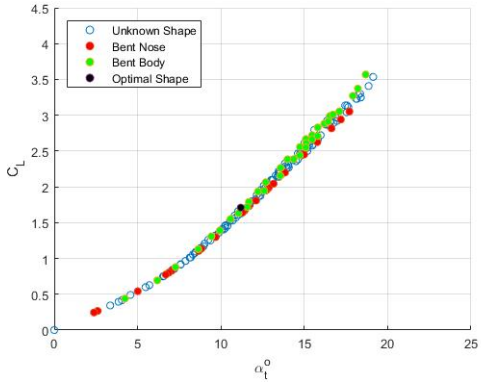

(c)

Fig. C-6 a) L/D, b) C_D, and c) C_L vs. α_t for Mach 3.0

List of Symbols, Abbreviations, and Acronyms

2-D	two-dimensional
3-D	three-dimensional
6-DOF	six degree of freedom
AFF	Air Force Finner
ARL	Army Research Laboratory
CCDC	US Army Combat Capabilities Development Command
CFD	computational fluid dynamics
CG	center of gravity
CREATE	Computational Research and Engineering Acquisition Tools and Environments
DOD	Department of Defense
fC	flowCart
L/D	lift-to-drag ratio
NASA	National Aeronautics and Space Administration
PSO	particle swarm optimization
RANS	Reynolds-averaged Navier–Stoke

Nomenclature

α	=	angle of attack, °
α_t	=	angle of attack at aerodynamic trim, °
α_T	=	total angle of attack, °
C_D	=	coefficient of drag, $\frac{D}{qS_{ref}}$
C_L	=	coefficient of lift, $\frac{L}{qS_{ref}}$
C_m	=	coefficient of pitching moment, $\frac{M}{qL_{ref}S_{ref}}$
C_{m_0}	=	coefficient of pitching moment at $\alpha = 0°$
C_p	=	pressure coefficient, $\frac{p-p_\infty}{q}$
D	=	aerodynamic drag, N, or projectile diameter, m
g	=	magnitude of acceleration due to gravity, m/s^2
L	=	aerodynamic lift, N
L/D	=	lift-to-drag ratio
L_{ref}	=	reference length, m
M	=	aerodynamic moment, $N - m$
p	=	static pressure, N/m^2
p_∞	=	freestream pressure, N/m^2
q	=	dynamic pressure, N/m^2
Q_1	=	location of first bend, mm
S_{ref}	=	reference area, m^2
$\phi_{1,2}$	=	first and second bending angle, °
θ	=	effective bending angle, °

1 (PDF) DEFENSE TECHNICAL INFORMATION CTR DTIC OCA

1 (PDF) CCDC ARL FCDD RLD DCI TECH LIB

2 (PDF) CCDC AC RDAR MEM A M DUCA G RODEBAUGH

1 (PDF) USAFA E STEPHEN

1 (PDF) USAFRL B DICKINSON

1 (PDF) AFOSR G ABATE

6 (PDF) CCDC AVMC FCDD AMS MMA J DOYLE K KENNEDY Z HALL M MCDANIEL C ROSEMA B WILKS

1 (PDF) JHU/APL A NEDUNGADI

31 (PDF) CCDC ARL FCDD RLW J ZABINSKI FCDD RLW A F FRESCONI FCDD RLW L W OBERLE P PEREGINO T SHEPPARD FCDD RLW LB N TRIVEDI E BYRD FCDD RLW LC J SADLER FCDD RLW LD A WILLIAMS M NUSCA A MCBAIN FCDD RLW LE J VASILE J BRYSON J DESPIRITO L STROHM J PAUL V BHAGWANDIN L FAIRFAX B GRUENWALD I CELMINS J SAHU B BURCHETT C MERMAGEN FCDD RLW LF M ILG B TOPPER D EVERSON T BROWN B NELSON FCDD RLW LH M MINNICINO R SUMMERS FCDD RLW ME S SILTON